DEVELOPMENT OF CHILD FINITE ELEMENT (FE) MODELS AND VEHICLE-TO-PEDESTRIAN COLLISION SIMULATIONS

Keisuke Ito
Mie Tokuyama
Hiroshi Miyazaki
Shigeki Hayashi
Yuichi Kitagawa
Tsuyoshi Yasuki
Toyota Motor Corporation
Japan

Paper Number 17-0279

ABSTRACT

This paper describes the development of child body finite element (FE) models and possible head injury mechanisms in vehicle-to-pedestrian collisions, while comparing the impact kinematics between child and adult models. Total Human Model for Safety (THUMS) Version 4 child models of 3-year-old (3YO), 6-year-old (6YO), and 10-year-old (10YO) were developed. The model geometry was generated based on computed tomography (CT) scan image data of actual pediatric subjects. The material properties of body components were defined for each model considering the age. Forty-eight vehicle-to-pedestrian collision simulations were conducted using three types of vehicle FE models (a sedan, SUV, and minivan), four sizes of pedestrian FE models (THUMS 3YO, 6YO, 10YO, and AM50) and four collision speeds (10, 20, 30, and 40 km/h). Strain based indicators were used for estimating head injuries such as skull fractures and brain injuries. The 3YO model predicted skull fracture in a collision with a SUV or minivan. Skull fractures were not observed with the other models. The child models commonly showed higher cumulative strain damage measure (CSDM) values in the brain compared to the AM50 model. Contact between the head of the child models and the front end of the hood generated stress concentration in the skull and resulted in skull fracture. The head angular acceleration of the child models increased after the shoulder contact. This high angular acceleration resulted in higher CSDM values in the brains of the child models.

INTRODUCTION

According to statistics published by the Japanese Ministry of Health, Labor and Welfare in 2014, traffic accidents accounted for 30% of fatal accidents in Japan involving children aged 15 years old or under. Statistics published in the same year by the National Police Agency of Japan showed that pedestrians accounted for the highest proportion (51%) of traffic accident fatalities involving children in the same age group (Figure 1). Furthermore, accident analysis carried out by Mizuno et al. (2005) [1] found that the head is the most common major injury location (37%) for fatalities and injuries (2-6 on the abbreviated injury scale (AIS), 462 people, excluding secondary impacts with the road surface) caused by accidents involving child pedestrians aged 15 or under (Figure 2). The probability of head injuries (2-6 on the maximum abbreviated injury scale (MAIS)) of this age group is also higher than the group aged 16 or over (Figure 3).

In addition to physique, the bodies of children have different mechanical properties and injury tolerances from adults, which result in different impact kinematics and injuries in car accidents. However, there are few studies that have investigated these differences in detail.

In the pedestrian safety assessment tests, the head injuries in vehicle collisions are evaluated using impactors. Although these tests use two types of head impactor with different weights to simulate a child and an adult, the impactors do not express the detailed anatomical features of the head. In addition, no full-body child pedestrian dummies have been developed.

Human body finite element (FE) models have been used in recent research into pedestrian impact kinematics and injuries, and various studies of child FE model development have been reported in the literature. Nishimura et al. (2002) [2] developed 6-year-old (6YO) and 9-year-old child FE models by scaling down an existing the Total Human Model for Safety (THUMS) Version 1 50th percentile American male (AM50) model.

Okamoto et al. (2003) [3] developed a 6YO child FE model using data from lower extremity magnetic resonance imaging (MRI) scans. Mizuno et al. (2005) [4] developed a 3-year-old (3YO) child model, again by scaling down the THUMS Version 1 AM50 model. Shen et al. (2016) [5] developed a 10-year old (10YO) child FE model using data from computed tomography (CT) and MRI scans. Meng et al. (2016) [6] also developed a 6YO child FE model by morphing an existing Global Human Body Modeling Consortium (GHBMC) 5th percentile American female model. Despite these developments, there are few studies of research using child FE models to study the whole body kinematics and head injuries of child pedestrians in vehicle collisions.

Therefore, the study described in this paper first developed child FE models that represent the anatomical structures and mechanical properties of children to enable the analysis of potential injuries suffered by child pedestrians. Next, the developed child FE models were used in vehicle-to-pedestrian collision simulations. This study then compares the whole body kinematics and head injury risk of these child models to those obtained using an adult male model with an average physique. Finally, this study discusses the head injury mechanisms for child pedestrians and the differences with the mechanisms for adults.

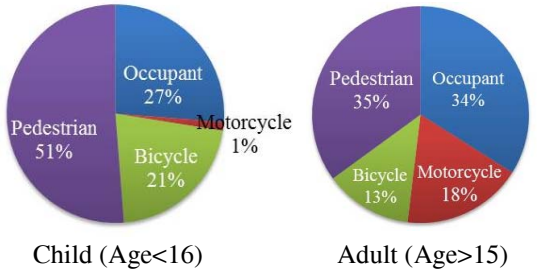

Figure 1. Proportions of traffic accident fatalities according to type.

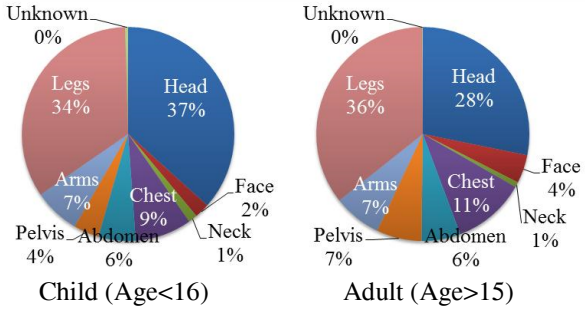

Figure 2. Proportions of injuries suffered by pedestrians according to body part.

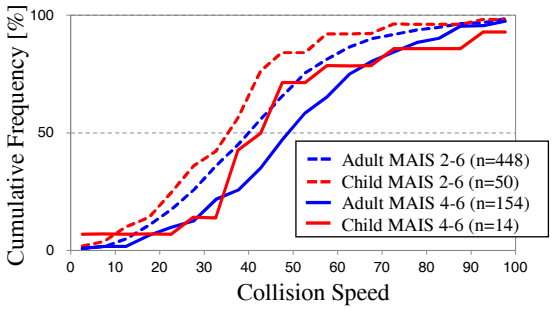

Figure 3. Cumulative distributions of head injuries.

MODEL DEVELOPMENT

Geometry Description

Figure 4 shows overall views of the THUMS Version 4 3YO, 6YO, and 10YO pedestrian models. The geometry of the body parts in the child models were generated using data from computed tomography (CT) scans. Geometry data was identified for each part such as the skin, bones, brain, and internal organs from high-resolution CT scans of 3-, 6-, and 10-year-old children with average physiques and converted into three-dimensional (3D) polygon data. This 3D polygon data was then fed into FE creation software to create solid and shell elements. The element length was set to between 3 to 5 mm.

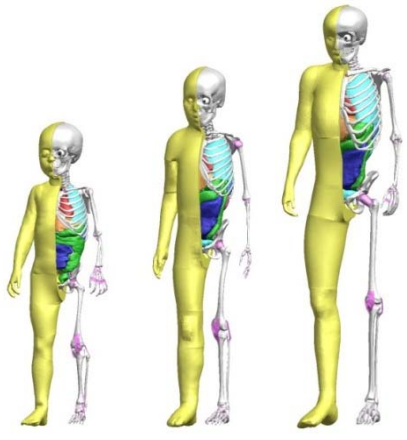

	3YO	6YO	10YO
Elements [k]	2,572	1,403	2,091
Nodes [k]	835	508	912
Height [cm]	94	118	138
Weight [kg]	15.5	24.3	35.0

Figure 4. Overall view of child body FE models.

Head and Neck Model

Figure 5 shows the 3YO head and neck models. The cerebrum, cerebellum, brain stem, and ventricle were modeled using solid elements, and the membranes covering the brain (i.e., the dura mater, subarachnoid, and pia mater) were modeled using shell elements. The cerebrum was expressed using a structure in which the left and right sides of the brain were connected by the corpus callosum. The head model also included a structure that links the brain stem and the spinal cord. The space between the brain and skull, and the cerebrospinal fluid that fills the ventricle were modeled using solid elements. The neck ligaments were modeled using shell elements and the neck muscles were modeled using beam and discrete elements. The cartilage at the end of the vertebra and the intervertebral disk between the vertebrae were modeled using solid elements.

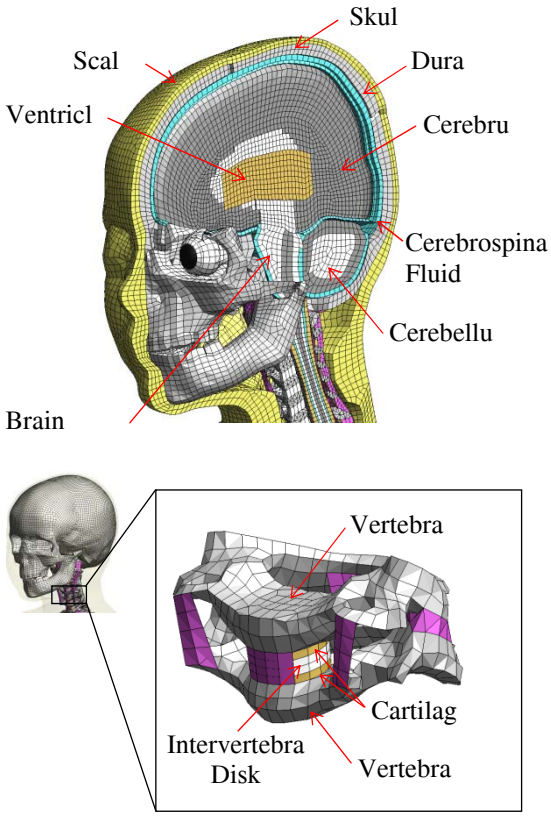

Figure 5. Head and neck models (3YO).

Torso Model

Figure 6 shows the 3YO torso model. Models of internal organs were located without any intervening gaps between the ribs and the pelvis (or the spine at the back of the model). The heart, liver, kidneys, spleen, pancreas, gallbladder, and bladder were modeled using solid elements, and the esophagus, stomach, duodenum, small intestine, and large intestine were modeled using shell elements. The lung surfaces were expressed using shell elements and the internal structures using solid elements. The artery and vena cava that travel from the heart close to the lungs and spine were modeled using shell elements. In addition, the membranes that cover the internal organs (i.e., the diaphragm, pleura, and peritoneum) were also modeled using shell elements. The connections and contacts between internal organs were defined based on anatomical data.

The pelvis consists of the iliac wing, ischium, and pubis. Cortical bones were modeled using shell elements and trabecular bones were modeled using solid elements. The triradiate cartilage that joins each section was modeled using solid elements.

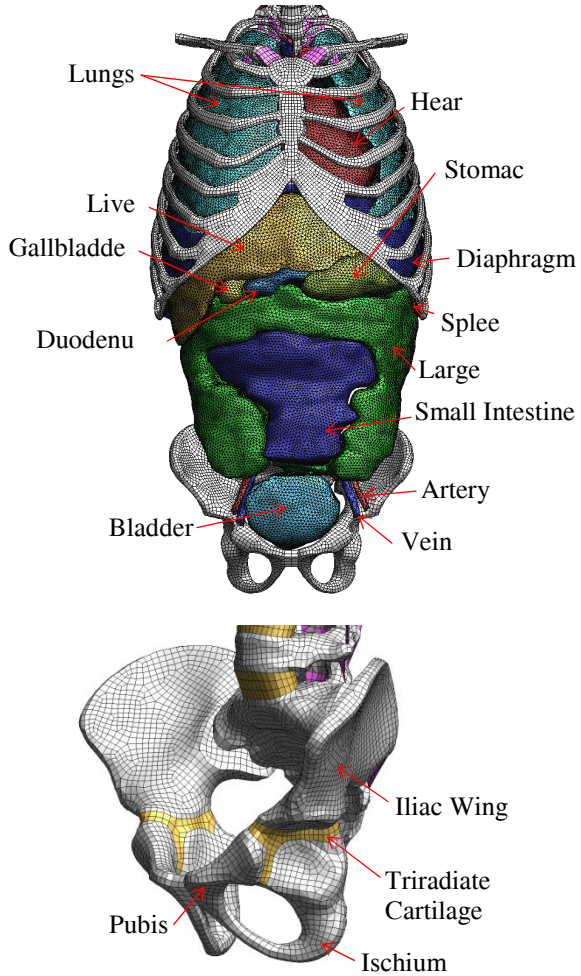

Figure 6. Torso model (3YO).

Extremity Model

Figure 7 shows the 3YO lower extremity model. The long bones (i.e., the femur, tibia, and fibula), were modeled using solid elements for both cortical and trabecular bones (the same approach was taken for the upper extremity model). For the other bones (such as the phalanges and the calcaneus), cortical bones were modeled using shell elements and trabecular bones were modeled using solid elements. One particular anatomical feature of lower extremities in children is the presence of growth plates and epiphyseal cartilage. These are mainly found at the end of the long bones and were modeled using solid elements to connect with the diaphyseal region.

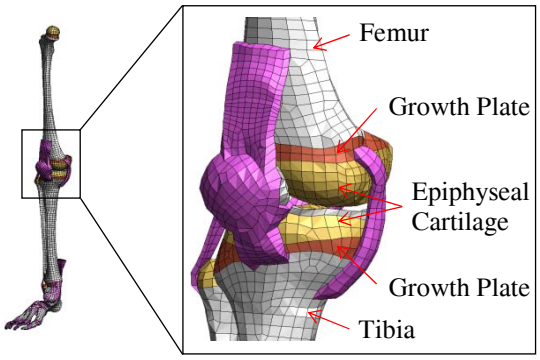

Figure 7. Lower extremity model (3YO).

Material Property

The material properties of each part of the human anatomy change in accordance with age. Currey et al. (1975) [7] carried out 3-point bending tests using femur cortical bones from subjects aged from 2 to 48 years old and identified the relationship between age and the young's modulus of the femur (Figure 8). This relationship was used to calculate the ratio of the young's modulus of the 3YO, 6YO, and 10YO child models with respect to an adult model (40YO) (3YO: 0.60, 6YO: 0.66, and 10YO: 0.72). Using these ratios, the material properties were scaled from the AM50 model to the child models. It was assumed that the same ratio can be used for bones other than the femur. However, since the specific effects of aging on other parts of the body apart from the bones were unknown, this study assumed the same material properties as adults.

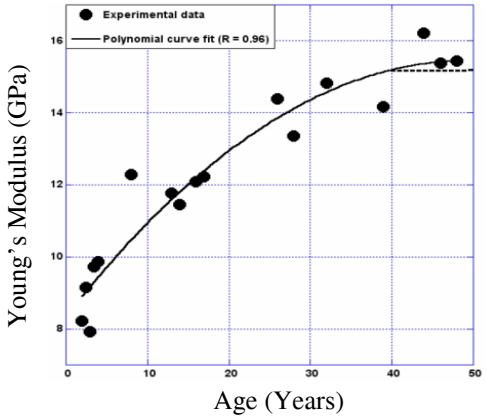

Figure 8. Relationship between age and Young's modulus of femur cortical bone.

McCalden et al. (1993) [8] carried out tensile tests using femur cortical bones from subjects aged 20 to 102 years old and identified the relationship between age and the fracture strain of the bone (Figure 9). The fracture strain of bones in the 3YO, 6YO, and 10YO child models were then estimated assuming that bones in children have the same relationship (3YO: 4.1%, 6YO: 4.0%, and 10YO: 3.9%). The same fracture strain was assumed for bones other than the femur (Table 1).

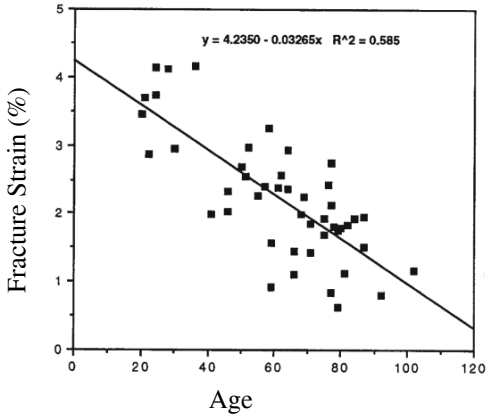

Figure 9. Relationship between age and fracture strain of femur cortical bone.

Table 1.
Assumed threshold values of cortical bone fracture strain.

Region	Indicator	Child			Adult (40YO)
		3YO	6YO	10YO	
Cortical Bone	Strain (%)	4.1	4.0	3.9	3.0

MODEL VALIDATION

The mechanical responses and whole-body kinematics of the completed child models were compared with test data obtained using post mortem human subjects (PMHS) and volunteers, as described in the literature [9-21]. The eleven load application cases shown in Table 2 were selected to validate the models. Each case used conditions that assume the load acting on a vehicle occupant or pedestrian in a vehicle collision. This paper describes the validation results of two cases: the head drop test carried out by Loyd et al. (2011) [9] and the femur 3-point bending test carried out by Ouyang et al. (2003) [15].

Table 2.
Child model validation cases.

Body Region	Loading Condition	Literature	Subject Age	Reference age for THUMS		
				3YO	6YO	10YO
Head	Lateral Compression	Loyd (2011)	0 - 67	-	-	9
	Drop	Loyd (2011)	0 - 67	-	-	9
Neck	Tension	Luck (2012)	0 - 18	-	-	9
Thorax	Anterior Impact	Ouyang (2006)	2 - 12	2 – 3	5 - 12	5 - 12
	Belt Loading	Kent (2009, 2011)	6 - 15	-	6 - 15	6 - 15
Abdomen	Belt Loading	Kent (2009, 2011)	6 - 15	-	6 - 15	6 - 15
Pelvis	Lateral Impact	Ouyang (2003)	2 - 12	2 – 4	5 - 12	5 - 12
Femur Tibia	3-point Bending	Ouyang (2003), Miltner (1989), Martin (1976), Stürtz (1980)	2 - 15	2 - 15	2 - 15	2 - 15
Whole Body	Low-speed Frontal Sled	Arbogast (2009)	6 - 30	-	6 - 9	8 - 12
	Low-speed Lateral Sled	Ita (2014)	6 - 8	-	6 - 8	-
	High-speed Frontal Sled	Ash (2009)	13	-	-	13

Head Drop Test

Figure 10 shows the model used for the simulated head drop test. The test was carried out using PMHS aged between 0 and 67 years old. In the test, the head was dropped freely onto an aluminum plate from a height of 30 cm so that the initial contact is on the side. The test recorded the loading response history when the impact occurred (measured using a load cell) and the acceleration response history of the head (measured using the weight of the head). This test was simulated using the 3YO, 6YO, and 10YO child models. Figure 11 compares the head acceleration history curve obtained in the test with those calculated using the child models. The head acceleration response of the 10YO child model approximately matched that obtained using a 9YO PMHS. Figure 12 compares the peak acceleration obtained in the test with those calculated using the child models. In the test results, the peak acceleration increased in accordance with age. The peak acceleration of the child models showed the same increasing trend.

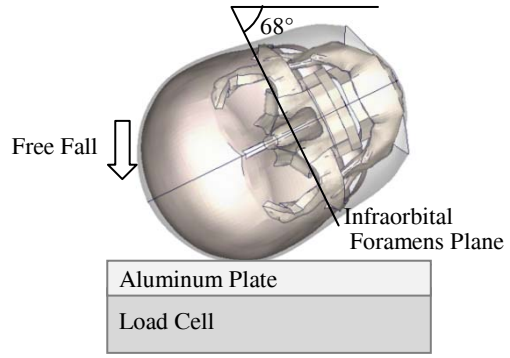

Figure 10. Head drop test (10YO).

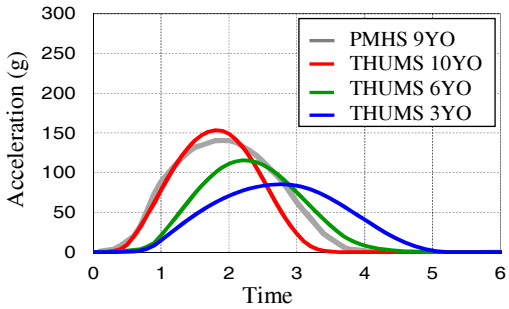

Figure 11. Comparison of head acceleration responses.

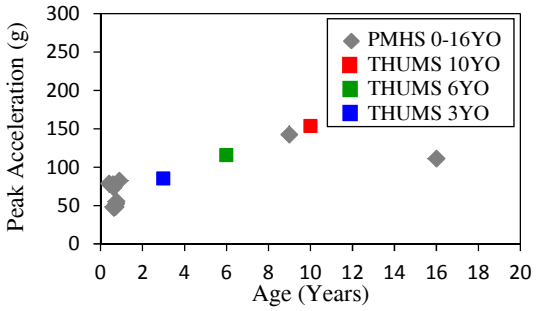

Figure 12. Relationship between age and peak acceleration.

Femur 3-point Bending Test

Figure 13 shows the model used for the simulated femur 3-point bending test. This test used PMHS aged between 2 and 15 years old. This was a quasi-static test in which the center of the femur was loaded using an impactor with a diameter of 20 mm. The bending moment when the bone fractured was calculated from the force and the displacement of impactor. This test was simulated using the 3YO, 6YO, and 10YO child models. The simulations determined that a bone fracture occurred if the strain values generated in the solid elements of the femur cortical bone reached the fracture strain values described above (Table 1). Figure 14 compares the bone fracture moment obtained in the test with those calculated using the child models. The bone fracture moments of the 3YO, 6YO, and 10YO child models were within the range of the test results. Furthermore, the bone fracture moments in the test increased in accordance with age. The bone fracture moments of the child models showed the same increasing trend. Based on the results, it was considered that the material properties and bone fracture criteria reference values defined for the bones in the child models were appropriate.

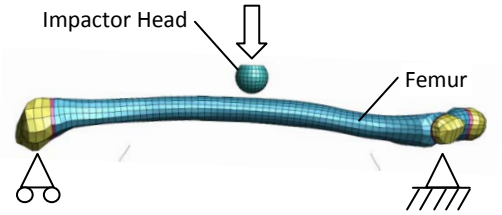

Figure 13. Femur 3-point bending test.

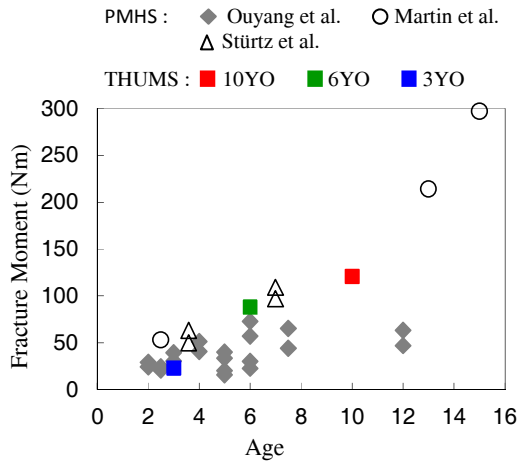

Figure 14. Relationship between age and femur fracture moment.

VEHICLE-TO-PEDESTRIAN COLLISION SIMULATION

Forty-eight vehicle-to-pedestrian collision simulations were carried out using the three developed child models and an AM50 model. Figure 15 outlines the models used in the simulations. Three different vehicle FE models were used: the sedan, SUV, and minivan models created by Watanabe et al. (2012) [22]. Pedestrians were simulated using four human FE models: the developed THUMS Version 4 3YO, 6YO, and 10YO child models, and the THUMS Version 4.02 AM50 model. The initial posture of the models was adjusted to the pedestrian posture described in SAE technical standards (2010) [23]. The collision speed was set to four levels: 10, 20, 30, and 40 km/h. The collision location was set to the center of the front vehicle surface in the width direction. The vehicle was directed to collide with the right side of the pedestrian. Table 3 lists the collision simulation conditions. LS-DYNA™ Version 971 was used for the simulations.

Five vehicle body parts were monitored as the contact locations with the pedestrian head: the grille (A), the leading edge of the hood (B), the top surface of the hood (C), the cowl (D), and the windshield glass (E). The impact speed when the head contacts the vehicle was expressed as the relative velocity between the head center of gravity and the vehicle. If the vehicle speed was defined as Vx and the speed of the pedestrian head as vx, vy, and vz, then the relative velocity between the head and the vehicle VR was obtained by Equation 1. In addition, Equation 2 was used to calculate the impact angle θ of the head.

$$|V_R| = \sqrt{(v_x - V_x)^2 + v_y{}^2 + v_z{}^2} \qquad \textbf{(Equation 1)}$$

$$\theta = \tan^{-1}\frac{v_z}{v_x - V_x} \qquad \textbf{(Equation 2)}$$

This study used an index based on bone and brain strain and an index based on the linear acceleration and angular velocity of the head center of gravity to estimate head injury (bone fractures and brain injury). The simulations assumed that a bone fracture occurred if the strain generated in the solid elements of the skull cortical bone exceeded the fracture strain values described above (Table 1). Brain injury (diffuse axonal injury: DAI) was estimated using the cumulative strain damage measure (CSDM) proposed by Takhounts et al. (2003) [24]. CSDM is an index used to assess the

occurrence of DAI based on the ratio of the volume of locations in which distortion in the brain exceeds a threshold value (25%) with respect to the volume of the whole brain. According to the brain injury risk curve derived by Takhounts et al. (2013) [25], a CSDM value of 49% was equivalent to a 50% probability of DAI (AIS4+). The head injury criterion (HIC15) was calculated to estimate injury caused by translational motion of the head. According to the skull fracture risk curve derived by Mertz et al. (1996) [26], an HIC15 value of 1,000 was equivalent to a 16% bone fracture probability. In addition, the brain injury criterion (BrIC) was calculated to estimate brain injury caused by rotational motion of the head. According to the brain injury risk curve derived by Takhounts et al. (2013) [25], a BrIC value of 0.89 is equivalent to a 30% probability of DAI (AIS4+).

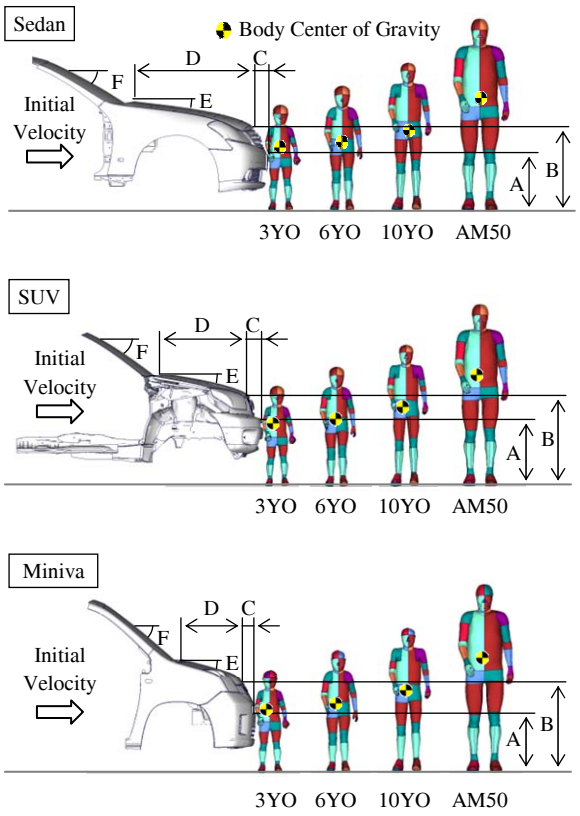

		Sedan	SUV	Minivan
A	Bumper Height [mm]	533	658	631
B	Hood Leading Edge [mm]	781	907	888
C	Bumper Protrusion [mm]	133	163	121
D	Hood Length [mm]	1142	861	493
E	Hood Inclination [deg]	5	9	14
F	Windshield Inclination [deg]	31	38	40

Figure 15. Simulation models of collisions between vehicle and pedestrian.

Table 3.
Simulate conditions.

Vehicle Type	Collision Speed [km/h]	Pedestrian Body Size			
		3YO	6YO	10YO	AM50
Sedan	10	Case 1	Case 5	Case 9	Case 13
	20	Case 2	Case 6	Case 10	Case 14
	30	Case 3	Case 7	Case 11	Case 15
	40	Case 4	Case 8	Case 12	Case 16
SUV	10	Case 17	Case 21	Case 25	Case 29
	20	Case 18	Case 22	Case 26	Case 30
	30	Case 19	Case 23	Case 27	Case 31
	40	Case 20	Case 24	Case 28	Case 32
Minivan	10	Case 33	Case 37	Case 41	Case 45
	20	Case 34	Case 38	Case 42	Case 46
	30	Case 35	Case 39	Case 43	Case 47
	40	Case 36	Case 40	Case 44	Case 48

RESULT

Collision with Sedan

Impact Kinematics Figure 16 shows the whole body kinematics in the pedestrian-to-sedan collisions at a collision speed of 40 km/h. With the 3YO child model, the pelvis contacted the bumper first. After the shoulder contacted the leading edge of the hood at 10ms after the collision, the head rotated laterally around the shoulder. The head finally contacted the top surface of the hood at 30 ms. With the 6YO child model, the upper femur contacted the bumper first. After the shoulder contacted the top surface of the hood at 40ms, the head rotated laterally around the shoulder. The head finally contacted the top surface of the hood at 60 ms. With the 10YO child model, the lower femur contacted the bumper first. After the pelvis contacted the leading edge of the hood at 30ms, the upper body fell down toward the front part of the hood. After the shoulder contacted the top surface of the hood at 50ms, the head rotated laterally around the shoulder. The head finally contacted the top surface of the hood at 70 ms. With the AM50 model, the knee contacted the bumper first. After the upper femur contacted the leading edge of the hood at 40ms, the body started rotating to the side around the pelvis. The lower extremities were thrust in the forward direction, the upper body fell down toward the middle part of the hood. After the shoulder contacted the top surface of

the hood at 130 ms followed by the head contacted the windshield glass at 140 ms.

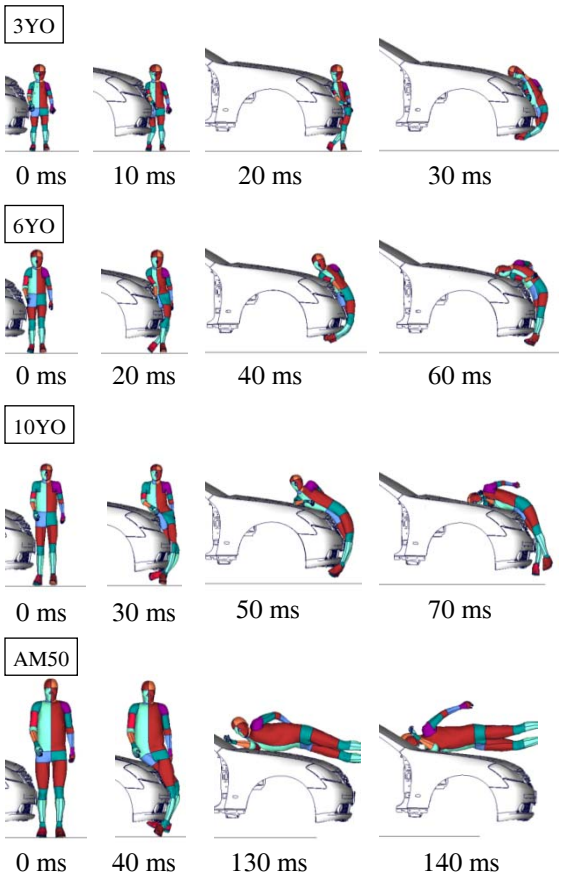

Figure 16. Pedestrian impact kinematics at a speed of 40km/h in collisions with sedan.

<u>Head Contact Condition</u> Table 4 shows the head contact time, contact location, impact velocity, impact angle, and peak contact force in the sedan collision simulations. Head contact time became later in accordance with age. The contact time of the 3YO child model was earlier than the other models and occurred after 30 ms at a collision speed of 40 km/h. The head of each child model contacted the top surface of the hood, regardless of the collision speed. With the AM50 model, the head contacted the top surface of the hood at collision speeds of 10 and 20 km/h. In contrast, the head contacted the cowl at 30 km/h and the windshield glass at 40 km/h. The collision angle of the head of the 3YO child model was smaller than the other models. The highest head contact velocity was generated by the 10YO child model at a collision speed of 40 km/h (13.5 m/s). Similarly, the highest peak contact force was also generated by the 10YO child model at a collision speed of 40 km/h (6.6 kN).

<u>Head Impact Response</u> Table 5 shows the skull fracture locations, brain CSDM, HIC15, BrIC, peak head linear acceleration, peak head angular velocity, and peak head angular acceleration in the sedan collision simulations. Bone fractures were not predicted in every case. The highest CSDM was generated by the 6YO child model at a collision speed of 40 km/h (80%). In the same case, the BrIC was 1.7, the peak angular velocity was 101 rad/s, and the peak angular acceleration was 10,728 rad/s^2.

Table 4.
Head contact conditions in collisions with sedan.

* A : Grille
B : Hood Leading Edge
C : Hood Top Surface
D : Cowl
E : Windshield Glass

	Collision Speed [km/h]	Contact Time [ms]	Contact Location*	Impact Velocity V_R [m/s]	Impact Angle θ [degree]	Peak Contact Force [kN]
3YO	10	90	C	2.4	59.2	1.7
	20	50	C	4.8	14.7	1.5
	30	40	C	7.9	5.9	1.7
	40	30	C	11.0	3.2	2.5
6YO	10	160	C	1.3	88.7	0.4
	20	100	C	3.6	97.9	1.4
	30	70	C	5.7	94.6	1.9
	40	60	C	7.8	77.5	2.0
10YO	10	210	C	3.2	75.0	0.6
	20	130	C	6.2	90.7	1.0
	30	100	C	9.0	81.6	3.4
	40	70	C	13.5	64.8	6.6
AM50	10	350	C	5.3	30.2	0.5
	20	230	C	6.5	74.2	1.8
	30	170	D	8.7	80.3	5.8
	40	140	E	12.1	70.9	4.4

Table 5.
Head responses in collisions with sedan.

	Collision Speed [km/h]	Skull Fracture	CSDM [%]	HIC15	BrIC	Peak Head Linear Acceleration [g]	Peak Head Angular Velocity [rad/s]	Peak Head Angular Acceleration [rad/s^2]
3YO	10	-	1	65	0.6	58	38	7,252
	20	-	3	140	1.2	50	69	7,471
	30	-	43	247	1.6	58	103	13,680
	40	-	66	438	2.0	83	130	20,695
6YO	10	-	0	4	0.5	15	30	1,577
	20	-	4	75	1.0	46	61	4,194
	30	-	46	201	1.4	66	87	6,577
	40	-	80	218	1.7	68	101	10,728
10YO	10	-	0	18	0.4	22	26	1,010
	20	-	0	52	0.9	35	47	2,682
	30	-	21	232	1.2	117	71	10,901
	40	-	77	987	1.7	225	95	20,705
AM50	10	-	0	3	0.3	14	16	390
	20	-	0	124	0.7	45	30	1,329
	30	-	11	1,025	1.0	148	44	7,710
	40	-	9	616	1.2	113	54	7,163

Collision with SUV

Whole Body Kinematics Figure 17 shows the whole body kinematics in the pedestrian-to-SUV collisions at a collision speed of 40 km/h. With the 3YO child model, the abdomen contacted the bumper first. After the shoulder contacted the grille at 10 ms after the collision, followed by the head contacted the leading edge of the hood at 20 ms. With the 6YO child model, the pelvis contacted the bumper first. After the shoulder contacted the leading edge of the hood at 20ms, the head rotated laterally around the shoulder. The head finally contacted the top surface of the hood at 40 ms. With the 10YO child model, the upper femur contacted the bumper first. After the abdomen contacted the leading edge of the hood at 20 ms, upper body fell down toward the front part of the hood. After the shoulder contacted the top surface of the hood at 50 ms, the head rotated laterally around the shoulder. The head finally contacted the top surface of the hood at 70 ms. With the AM50 model, the knee contacted the bumper first. After the pelvis contacted the leading edge of the hood at 30 ms, the upper body fell down toward the middle part of the hood. After the shoulder contacted the top surface of the hood at 100ms, followed by the head contacted the windshield glass at 110 ms.

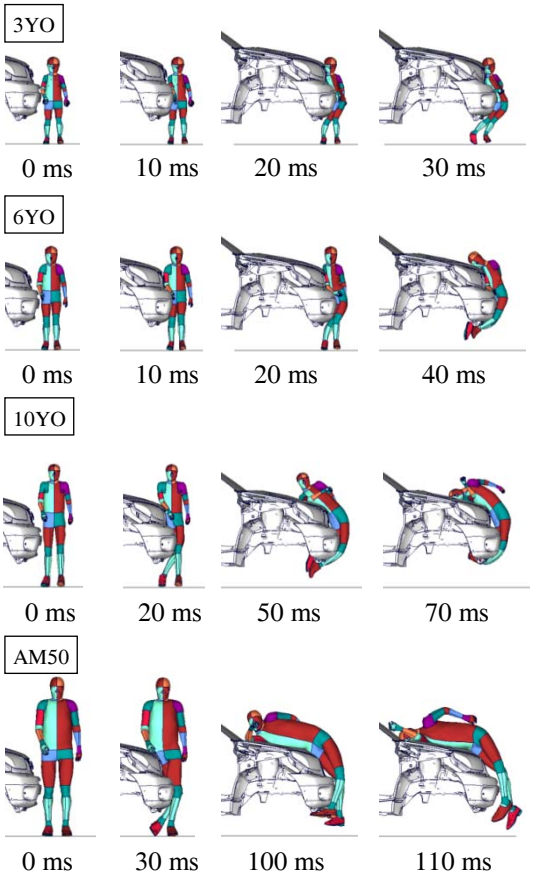

Figure 17. Pedestrian impact kinematics at a speed of 40km/h in collisions with SUV.

Head Contact Condition Table 6 shows the head contact time, contact location, impact velocity, impact angle, and peak contact force in the SUV collision simulations. In the same way as the sedan collision simulations, head contact time became later in accordance with age. The contact time of the 3YO child model was earlier than the other models and occurred after 20 ms at a collision speed of 40 km/h. With the 3YO child model, the head contacted the grille at a collision speed of 10 km/h and the leading edge of the hood at collision speeds of 20 km/h and above. The head of the 6YO child model contacted the top surface of the hood, regardless of the collision speed. At a collision speed of 10 km/h, the head of the 10YO child model did not contact the vehicle. At collision speeds of 20 km/h and above, the head contacted the top surface of the hood. Similarly, the head of the AM50 model did not contact the vehicle at a collision speed of 10 km/h. With the AM50 model, the head contacted the top surface of the hood at a collision speed of 20 km/h, the cowl at 30 km/h, and the windshield glass at 40 km/h. In the same way as the sedan collision simulations, the collision angle of the head of the 3YO child model was smaller than the other models. The highest head contact velocity was generated by the 10YO child model at a collision speed of 40 km/h (12.1 m/s). However, the highest head contact force was generated by the 3YO child model at a collision speed of 40 km/h (6.5 kN).

Head Impact Response Table 7 shows the skull fracture locations, brain CSDM, HIC15, BrIC, peak head linear acceleration, peak head angular velocity, and peak head angular acceleration in the SUV collision simulations. A skull fracture (temporal bone) was predicted with the 3YO child model at a collision speed of 40 km/h. In the same case, the HIC15 was 2,613 and the peak linear acceleration was 221 g. The highest CSDM was generated by the 6YO child model at a collision speed of 40 km/h (85%). In the same case, the BrIC was 1.4, the peak angular velocity was 87 rad/s, and the peak angular acceleration was 16,900 rad/s^2.

Table 6.
Head contact conditions in collisions with SUV.

* A : Grille
B : Hood Leading Edge
C : Hood Top Surface
D : Cowl
E : Windshield Glass

	Collision Speed [km/h]	Contact Time [ms]	Contact Location*	Impact Velocity V_R [m/s]	Impact Angle θ [degree]	Peak Contact Force [kN]
3YO	10	80	A	2.2	37.8	0.5
	20	40	B	5.6	9.0	3.0
	30	30	B	8.4	3.1	4.6
	40	20	B	11.1	1.1	6.5
6YO	10	130	C	1.1	100.9	0.2
	20	70	C	3.6	77.7	3.1
	30	50	C	5.7	62.5	4.3
	40	40	C	7.3	56.9	5.4
10YO	10	-	-	-	-	-
	20	120	C	4.6	105.0	0.9
	30	80	C	7.8	90.5	2.3
	40	70	C	12.1	67.9	6.2
AM50	10	-	-	-	-	-
	20	190	C	6.1	87.2	5.2
	30	140	D	10.2	82.7	5.5
	40	110	E	11.7	87.1	5.2

Table 7.
Head responses in collisions with SUV.

	Collision Speed [km/h]	Skull Fracture	CSDM [%]	HIC15	BrIC	Peak Head Linear Acceleration [g]	Peak Head Angular Velocity [rad/s]	Peak Head Angular Acceleration [rad/s^2]
3YO	10	-	0	14	0.4	19	28	2,718
	20	-	0	495	0.5	104	30	5,037
	30	-	4	1,195	0.7	155	40	9,288
	40	Temporal Bone	15	2,613	0.8	221	47	11,303
6YO	10	-	0	1	0.6	8	36	2,266
	20	-	43	150	1.1	106	63	9,897
	30	-	72	424	1.2	147	73	12,706
	40	-	85	634	1.4	183	87	16,900
10YO	10	-	0	-	0.4	13	25	1,347
	20	-	0	30	0.9	32	52	3,225
	30	-	24	133	1.4	80	120	8,695
	40	-	74	1,010	1.8	210	278	19,540
AM50	10	-	0	-	0.4	5	5	600
	20	-	0	586	0.7	131	131	8,538
	30	-	62	1,262	1.0	140	143	8,944
	40	-	65	818	1.8	116	168	15,689

Collision with Minivan

Whole Body Kinematics Figure 18 shows the whole body kinematics in the pedestrian-to-minivan collisions at a collision speed of 40 km/h. The impact kinematics, contact locations, and contact times of the child models were the same as in the SUV collision simulations. With the AM50 model, the knee contacted the bumper first. After the pelvis contacted the leading edge of the hood at 30 ms after the collision, the upper body fell down toward the rear part of the hood. After the shoulder contacted the windshield glass at 90 ms, followed by the head contacted the same parts at 110 ms.

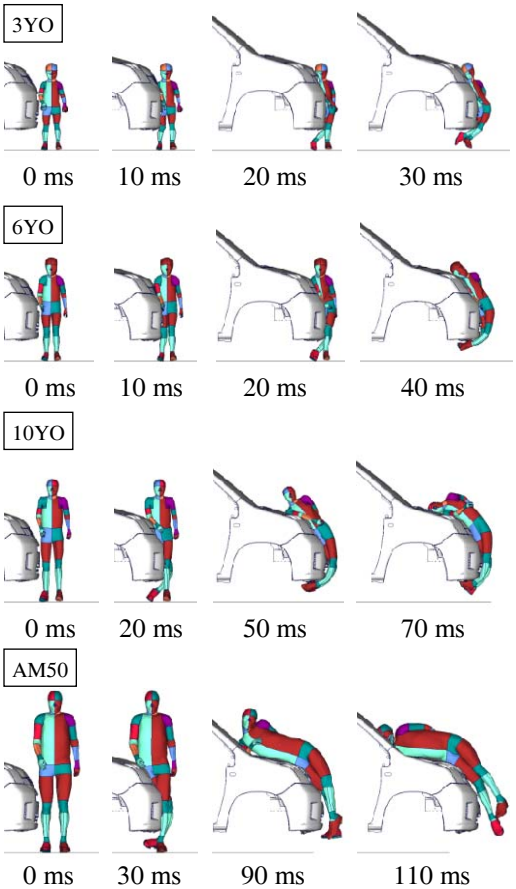

Figure 18. Pedestrian Impact kinematics at a speed of 40km/h in collisions with minivan.

Head Contact Condition Table 8 shows the head contact times, contact locations, impact velocities, impact angles, and peak contact forces in the minivan collision simulations. In the same way as the collision simulations involving the other vehicle types, head contact time became later in accordance with age. The contact time of the 3YO child model was earlier than the other models and occurred after 20 ms at a collision speed of 40 km/h. With the 3YO child model, the head contacted the grille at a collision speed of 10 km/h and the leading edge of the hood at collision speeds of 20 km/h and above. The head of the 6YO and 10YO child models contacted the top surface of the hood, regardless of the collision speed. At a collision speed of 10 km/h, the head of the AM50 model did not contact the vehicle. With the AM50 model, the head contacted the windshield glass at collision speeds of 20 km/h and above. In the same way as the collision simulations involving the other vehicle types, the collision angle of the head of the 3YO child model was smaller than the other models. The highest head contact velocity was generated by the AM50 model at a collision speed of 40 km/h (15.9 m/s). However, the highest head contact force was generated by the 10YO child model at a collision speed of 40 km/h (3.8 kN).

Head Impact Response Table 9 shows the skull fracture locations, brain CSDM, HIC15, BrIC, peak head linear acceleration, peak head angular velocity, and peak head angular acceleration in the minivan collision simulations. Skull fractures (temporal bone and mandible) were predicted with the 3YO child model at a collision speed of 40 km/h. In the same case, the HIC15 was 835 and the peak linear acceleration was 108 g. The highest CSDM was generated by the 6YO child model at a collision speed of 40 km/h (78%). In the same case, the BrIC was 1.4, the peak angular velocity was 83 rad/s, and the peak angular acceleration was 14,215 rad/s^2.

* A : Grille
B : Hood Leading Edge
C : Hood Top Surface
D : Cowl
E : Windshield Glass

Table 8.
Head contact conditions in collisions with minivan.

	Collision Speed [km/h]	Contact Time [ms]	Contact Location	Impact Velocity V_R [m/s]	Impact Angle θ [degree]	Peak Contact Force [kN]
3YO	10	80	A	2.1	43.6	0.9
	20	40	B	5.2	6.9	1.5
	30	30	B	8.2	2.7	2.0
	40	20	B	11.1	1.5	3.2
6YO	10	120	C	1.6	82.5	0.6
	20	70	C	3.9	70.8	2.0
	30	50	C	6.4	39.6	2.8
	40	40	C	9.7	19.6	3.2
10YO	10	190	C	1.6	89.6	0.4
	20	120	C	4.3	98.8	1.2
	30	80	C	8.2	75.7	2.6
	40	70	C	11.4	66.8	3.8
AM50	10	-	-	-	-	-
	20	180	E	7.2	71.0	1.3
	30	130	E	12.5	49.6	1.8
	40	110	E	15.9	41.8	3.3

Table 9.
Head responses in collisions with minivan.

	Collision Speed [km/h]	Skull Fracture	CSDM [%]	HIC15	BrIC	Peak Head Linear Acceleration [g]	Peak Head Angular Velocity [rad/s]	Peak Head Angular Acceleration [rad/s^2]
3YO	10	-	0	19	0.5	32	30	3,530
	20	-	0	135	0.7	50	42	4,529
	30	-	14	376	1.0	67	63	10,290
	40	Zygomatic Bone Mandible	33	835	1.1	108	72	13,241
6YO	10	-	0	9	0.6	22	32	2,707
	20	-	36	158	1.0	67	57	8,004
	30	-	62	362	1.1	94	65	11,214
	40	-	78	824	1.4	109	83	14,215
10YO	10	-	0	5	0.5	15	27	1,607
	20	-	0	50	0.9	41	55	3,911
	30	-	31	217	1.4	89	88	10,117
	40	-	55	503	1.7	129	107	14,041
AM50	10	-	0	-	0.3	-	18	500
	20	-	0	31	0.6	33	33	2,461
	30	-	2	41	0.9	46	54	2,991
	40	-	16	80	1.0	85	103	2,992

DISCUSSION

Kinematic

The impact kinematics by which the models fell down toward the vehicle differed because the child and AM50 models in a pedestrian posture have different center of gravity heights with respect to the leading edge of the hood. With the 3YO and 6YO child models, body parts higher than the center of gravity (i.e., the thorax, shoulder, and head) contacted the leading edge of the hood. The upper body of these models deformed along the shape of the front vehicle surface and the upper body did not fall down toward the hood. The head of the models contacted locations close to the front of the hood. With the 10YO child model, the body part at the center of gravity position (i.e., the pelvis) contacted the leading edge of the hood. The body upward from the pelvis then fell down toward the front part of the hood. The head of the model contacted locations close to the middle part of the hood. With the AM50 model, the femur below the center of gravity position contacted the leading edge of the hood. The lower extremities were thrust in the forward direction of the vehicle and the body rotated toward the rear of the vehicle centered on the pelvis. Subsequently, the upper body fell down toward either the middle part or the rear part of the hood. The head contacted either the rear part of the hood or the windshield glass.

Head Contact Condition

The head contact force of the child models was higher than the AM50 model. The causes of this result are discussed below. In the sedan and minivan collision simulations, the highest head contact force occurred with the 10YO child model at a collision speed of 40 km/h. In the sedan collision simulations, the pelvis of the 10YO child model contacted the leading edge of the hood at 30 ms after the collision. Then, the upper body fell down toward the hood and the head moved downward. The velocity of the head in the Z direction rose, thereby increasing the relative velocity between the head and the vehicle (red line in Figure 19). As a result, the head contact velocity at the point of contact (70 ms) was 13.5 m/s, higher than the other models. This is the probable cause of the high contact force. In the minivan collision simulations, the head contact velocity of the 10YO child model is lower than the AM50 model. However, the head contact force of the 10YO child model is higher than the AM50 model probably because the head of the AM50 model contacted the windshield. In the SUV collision simulations, the highest head contact force occurred with the 3YO child model. This is assumed to be because the head contact angle of the 3YO child model was smaller than the other models, which caused the head to contact the vehicle from the front of the leading edge of the hood.

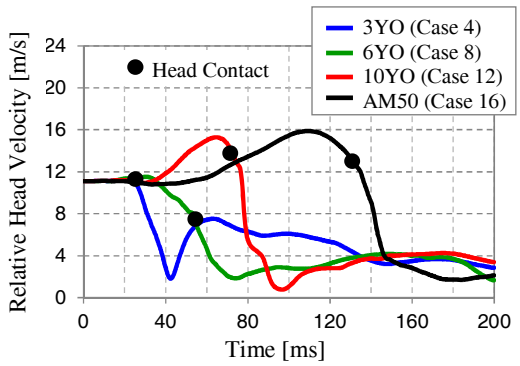

Figure 19. Relative head velocity curves with respect to vehicle at a speed of 40km/s in collisions with sedan.

Head Injury Indicator Values

In the SUV and minivan collision simulations, the skull strain of the 3YO child model exceeded the fracture strain at a collision speed of 40 km/h. The head of this model contacted the vehicle from the front of the leading edge of the hood. This probably resulted in concentrated higher force application to the head compared to cases in which the head contacted the vehicle from the top surface of the hood. This resulted in high stress generation at the contact location and higher skull strain (Figure 20). In contrast, the skull strain of the AM50 model did not exceed the fracture strain. Therefore, the skull strain of the 3YO child model was higher than the AM50 model probably because the head of the 3YO child model contacted the leading edge of the hood from the front of the vehicle.

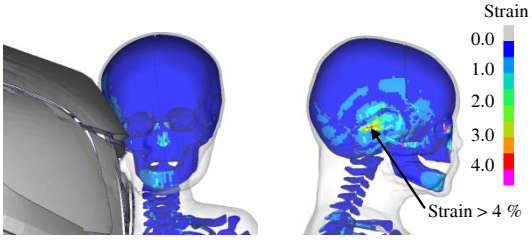

Figure 20. Skull strain contour of 3YO child model at a speed of 40km/h in collisions with SUV (Case 20).

The highest CSDM value was generated in the collision between the 6YO child model and the SUV at a collision speed of 40 km/h. The shoulder of the 6YO child model contacted the leading edge of the hood at 20 ms after the collision. The shoulder was forcibly pushed away, which generated a large velocity difference between the head and thorax. This caused the head to rotate rapidly centered on the shoulder. The angular acceleration then increased as the angular velocity of the head rose suddenly (green line in Figure 21). This increase in angular acceleration probably caused high brain strain before contact between the head and the hood (Figure 22). Subsequently, the head contacted the hood at 40 ms, which suppressed the rotation and caused the angular velocity to decrease rapidly. The brain strain then increased further because the rotation of the brain did not stop at the same time as the skull. The pelvis of the AM50 model contacted the leading edge of the hood at 20 ms. The head rotated around the pelvis until the point of contact between the shoulder and the hood (100 ms) (Figure 23). The radius of rotation of the head in the AM50 model was larger than the 6YO child model, which means that the time from the start of head rotation to the contact with the hood was longer (6YO child model: 20 ms, AM50: 80 ms). This is the probable reason why the gradient of the head angular velocity of the AM50 model is smaller than the 6YO child model. As a result, it is likely that the brain strain is higher than the AM50 model due to the rapid head rotation that occurs between the shoulder of the 6YO child model contacting the leading edge of the hood and the head contacting the vehicle.

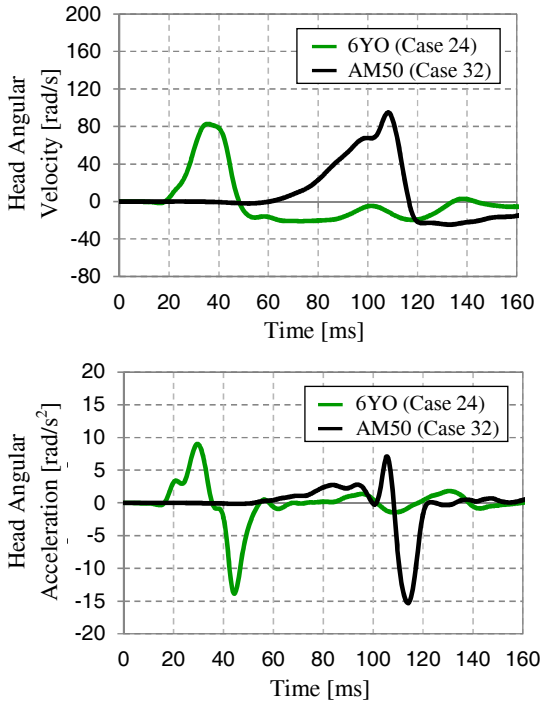

Figure 21. Head angular velocity and acceleration curves of 6YO child model and AM50 model at a speed of 40km/h in collisions with SUV.

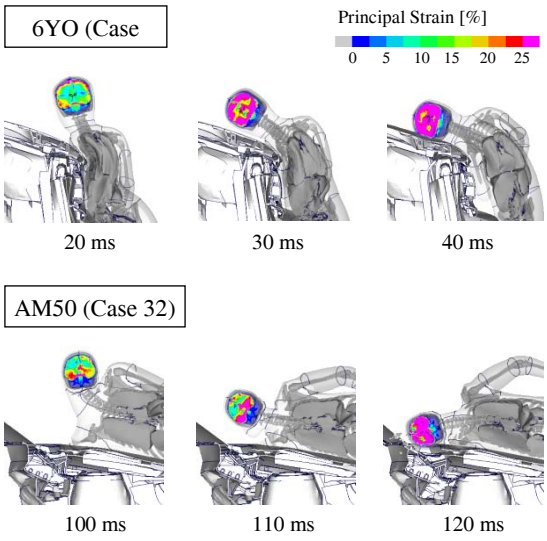

Figure 22. Brain principal strain contours of 6YO child model and AM50 model at a speed of 40km/h in collisions with SUV.

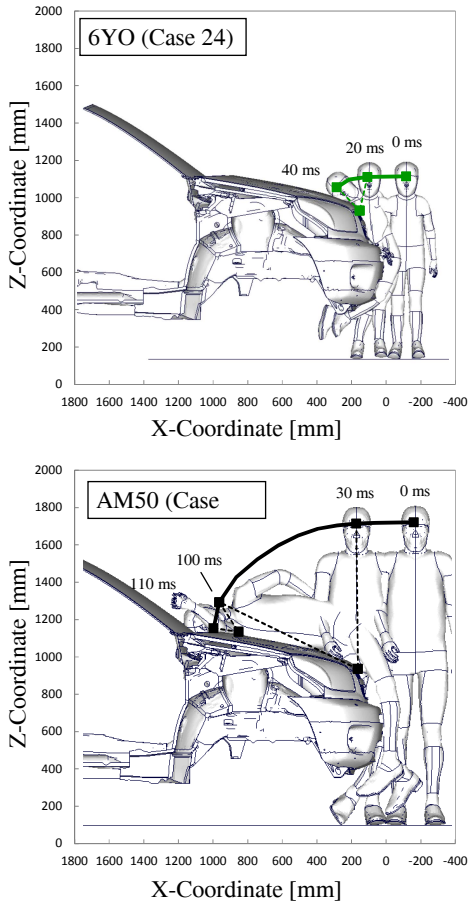

Figure 23. Head trajectories of 6YO child model and AM50 model at a speed of 40km/h in collisions with SUV.

Figure 24 shows the relationship between collision speed and CSDM. The CSDM of the child models increased in accordance with the collision speed. At collision speeds of 30 km/h and above, the CSDM exceeded 49% (DAI probability: 50%) in some cases with both the child and AM50 models.

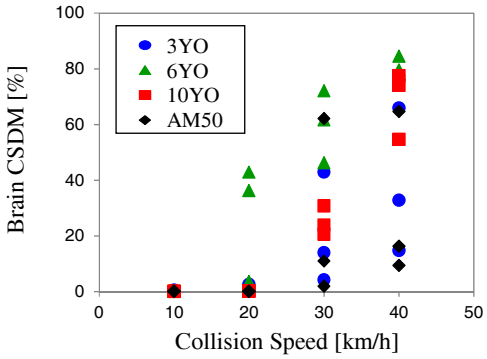

Figure 24. Relationship between collision speed and CSDM Values.

LIMITATION

This study carried out 48 vehicle-to-pedestrian collision simulations under different vehicle (sedan, SUV, and minivan), pedestrian physique (3YO, 6YO, 10YO, and AM50 models), and collision speed (10, 20, 30, and 40 km/h) conditions. The simulation results found different injury trends for children and adults. However, actual accident conditions are more varied than these simulations, and these results can only predict possible outcomes in certain scenarios. Further study is needed to analyze the child head injury mechanisms and to understand the differences with adult injury mechanisms.

This study also evaluated the possibility of bone fractures and brain injuries based on assumed threshold values. The bone fracture threshold values for children were assumed based on the effects of aging on femur durability described in the literature, and these assumptions were also applied to the skull. However, the injury tolerance of bones probably varies depending on the part of the body. The threshold value for strain that was used to calculate the CSDM value was assumed to be the same as the threshold value adopted in the AM50 model (25%). However, the actual brain injury tolerance probably varies with age. Future study must consider the effects of body location and age on these threshold values.

CONCLUSIONS

THUMS Version 4 child models were developed representing the anatomical structures of 3YO, 6YO, and 10YO children. In each model, the geometries of the skeleton, brain, and internal organs were precisely represented based on data from high-resolution CT scans. The material properties of the child models were defined considering the aging effects described in the literature. The mechanical responses and whole-body kinematics of the child models were compared with test results obtained using PMHS and volunteers, as described in the literature. The mechanical responses of the child models (e.g., the impact response of the head) approximately matched the experimental results.

Forty-eight vehicle-to-pedestrian collision simulations were carried out under different vehicle (sedan, SUV, and minivan), pedestrian physique (3YO, 6YO, 10YO, and AM50 models), and collision speed (10, 20, 30, and 40 km/h) conditions. The whole body kinematics and head injuries of the child and AM50 models were compared in vehicle-to-pedestrian collisions.

The simulation results of all 48 cases indicated that the skull and brain strain values of the child models were higher than the AM50 model in the following cases, even under the same collision conditions. In the SUV and minivan collision simulations, the head of the 3YO child model struck the leading edge of the hood firmly in some cases. This caused concentrated high force application to the side of the head, resulting in higher skull strain than the AM50 model. In addition, in the SUV collision simulations, the shoulder of the 6YO child model was pushed strongly into the leading edge of the hood in some cases. The subsequent rapid rotation of the head generated high angular acceleration, resulting in higher brain strain than the adult model. These phenomena are probably one reason why the head injury rate of children is higher than that of adults.

REFERENCES

[1] Mizuno, Y. 2005. “Summary of IHRA Pedestrian Safety WG Activities (2005) - Proposed Test Methods to Evaluate Pedestrian Protection Afforded by Passenger Cars.” 19th International technical Conference on the Enhanced Safety of Vehicles (ESV), 05-0138.

[2] Nishimura, R., Hasegawa, J. 2002. “Development of the Human FEM Model for Child Pedestrian.” JSAE 20025504.

[3] Okamoto, M., Takahashi, Y., Mori, F., Hitosugi, M., Madeley, J., Iverson, J., Crandall, J. 2003. “Development of Finite Element Model for Child Pedestrian Protection.” 18th ESV, 151

[4] Mizuno, K., IwataK., Deguchi, T., Ikami, T., Kubota, M. 2005. “Development of Three-Year Old Child Human FE Model.” Traffic Injury Prevention, 6(4), 361-371

[5] Shen, M., Mao, H., Jiang, B., Zhu, F., Jin, X., Dong, L., Ham, S.J., Palaniappan, P., Chou, C., Yang, K. 2016. “Introduction of Two New Pediatric Finite Element Models for Pedestrian and Occupant Protections.” SAE 2016-01-1492.

[6] Meng, Y., Guleyupoglu, B., Koya, B., Gayzik, S., Untaroiu, C.D. 2016. “A 6 Year-Old Pediatric Finite Element Model for Simulating Pedestrian Impacts.” 14th International LS-DYNA User Conference.

[7] Currey, J., Butler, G. 1975. “The Mechanical Properties of Bone Tissue in Children.” The Journal of Bone and Joint Surgery, 57(6), 810-814.

[8] McCalden, R., McGeough, J., Barker, M., Cort-Brown, C. 1993. “Age-Related Changes in the Tensile Properties of Cortical Bone.” The Journal of Bone and Joint Surgery, 75(8), 1193-1205.

[9] Loyd, A.M. 2011. “Studies of the Human Head From Neonate to Adult: an Inertial, Geometrical and Structural Analysis with Comparisons to the ATD Head [Ph.D. Dissertation].” Department of Biomedical Engineering, Duke University, Durham, NC, USA.

[10] Luck, J.F., Nightingale, R.W., Song, Y., Kait J.R., Loyd, A.M., Myersm B.S., Bass, C.R. 2012. “Tensile Failure Properties of the Perinatal, Neonatal, and Pediatric Cadaveric Cervical Spine.” SPINE, 38(1), E1-E12.

[11] Ouyang, J., Zhao, W., Xu, Y., Chen, W., Zhong, S. 2006. “Thoracic Impact Testing of Pediatric Cadaveric Subjects.” The Journal of Trauma. 61, 1492-1500.

[12] Kent, R., Salzar, R., Kerrigan, J., Parent, D., Lessley, D., Sochor M., Luck J.F., Loyd A., Song, Y., Nighitingale, R., Bass, C.R., Maltese, M.R. 2009. "Pediatric Thoracoabdominal Biomechanics." Stapp Car Crash Journal, 53, 373-401.

[13] Kent, R., Lopez-Valdes, F., Lamp, J., Lau, S, Parent, D., Kerrigan, J., Lessley, D., Salzar, R. 2011. "Characterization of the Pediatric Chest and Abdomen using Three Post-Mortem Human Subjects." 22nd ESV, 11-0394.

[14] Ouyang, J., Zhu, Q., Zhao, W., Xu, Y., Chen, W., Zhong, S. 2003. "Experimental Cadaveric Study of Lateral Impact of the Pelvis in Children." Journal of First Military Medical University. 23(5), 397-401.

[15] Ouyang, J., Zhu, Q., Zhao, W., et al. 2003. " Biomechanical Character of Extremity Long Bones in Children and its Significance." Chinese Journal of Clinical Anatomy, Vol.21, No.6, pp.620-623

[16] Miltner, E., Kallieris, D. 1989. "Quasistatische und dynamische Biegebelastung des kindlichen Oberschenkels zur Erzeugung einer Femurfraktur." Zeitschrift für Rechtsmedizin, 102(8), 535-544.

[17] Martin, R., Atkinson, P. 1976. "Age and Sex-Related Changes in the Structure and Strength of Human Femoral Shaft." Journal of Biomechanics, 10, 223-31.

[18] Stürtz, G. 1980. "Biomechanical Data of Children." SAE Paper 801313.

[19] Arbogast, K.B., Balasubramanian, S., Seacrist, T., Maltese, M.R., García-España, J.F., Hopely, T., Constans, E., Lopez-Valdes, F.J., Kent, R.W., Tanji, H., Higuchi, K. 2009. "Comparison of Kinematic Responses of the Head and Spine for Children and Adults in Low-Speed Frontal Sled Tests." Stapp Car Crash Journal, 53, 329-372, SAE Paper 2009-22-0012.

[20] Ita, M., Seacrist, T., Dahle, E., Bolte, J., Kang, Y. 2014. "Comparison of Q3s ATD Biomechanical Responses to Pediatric Volunteers." Ohio State University Injury Biomechanics Symposium.

[21] Ash, J., Abdelilah, Y., Crandall, J., Parent, D., Sherwood, C., Kallieris, D. 2009. "Comparison of Anthropomorphic Test Dummies with a Pediatric Cadaver Restrained by a Three-Point Belt in Frontal Sled Tests." 21st ESV, 09-0362.

[22] Watanabe, R., Katsuhara, T., Miyazaki, H., Kitagawa, Y., Yasuki, T. 2012. "Research of the Relationship of Pedestrian Injury to Collision Speed, Car-Type, Impact Location and Pedestrian Sizes using Human FE Model(THUMS Version 4)." Stapp Car Crash Journal, 56, 269-321.

[23] Performance Specifications for a Midsize Male Pedestrian Research Dummy. 2010. Surface Vehicle Information Report, SAE J2782 OCT2010.

[24] Takhounts, E.G., Eppinger, R.H., Campbell, J.Q., Tannous, R.E., Power, E.D., Shook, L.S. 2003. "On the Development of the SIMon Finite Element Head Model." Stapp Car Crash Journal, 47, 107-133.

[25] Takhounts, E.G., Craig, M.J., Moorhouse, K., McFadden, J., Hasija, V. 2013. "Development of Brain Injury Criteria (BrIC)." Stapp Car Crash Journal, 57, 243-266.

[26] Mertz, H.J., Prasad, P., Nusholtz, G. 1996. "Head Injury Risk Assessment for Forehead Impacts." SAE 960099, 26-46.